MAGNETIZED NEUTRON STAR ATMOSPHERES: BEYOND THE COLD PLASMA APPROXIMATION

V. F. Suleimanov[1,2], G. G. Pavlov[3,4], and K. Werner[1]

ABSTRACT

All the neutron star (NS) atmosphere models published so far have been calculated in the "cold plasma approximation", which neglects the relativistic effects in the radiative processes, such as cyclotron emission/absorption at harmonics of cyclotron frequency. Here we present new NS atmosphere models which include such effects. We calculate a set of models for effective temperatures $T_{\rm eff} = 1$–3 MK and magnetic fields $B \sim 10^{10}$–10^{11} G, typical for the so-called central compact objects (CCOs) in supernova remnants, for which the electron cyclotron energy $E_{c,e}$ and its first harmonics are in the observable soft X-ray range. Although the relativistic parameters, such as $kT_{\rm eff}/m_e c^2$ and $E_{c,e}/m_e c^2$, are very small for CCOs, the relativistic effects substantially change the emergent spectra at the cyclotron resonances, $E \approx sE_{c,e}$ ($s = 1, 2, \ldots$). Although the cyclotron absorption features can form in a cold plasma due to the quantum oscillations of the free-free opacity, the shape and depth of these features change substantially if the relativistic effects are included. In particular, the features acquire deep Doppler cores, in which the angular distribution of the emergent intensity is quite different from that in the cold plasma approximation. The relative contributions of the Doppler cores to the equivalent widths of the features grow with increasing the quantization parameter $b_{\rm eff} \equiv E_{c,e}/kT_{\rm eff}$ and harmonic number s. The total equivalent widths of the features can reach ~ 150–250 eV; they increase with growing $b_{\rm eff}$ and are smaller for higher harmonics.

Subject headings: radiative transfer — stars: neutron — stars: magnetic fields — pulsars: individual (1E 1207.4-5209, PSR J1210–5226, PSR J1852+0040, PSR J0821–4300)

1. INTRODUCTION

Thanks to the high sensitivity and spectral resolution of the X-ray observatories *Chandra* and *XMM-Newton*, absorption features in thermal spectra of the so-called X-ray dim isolated neutron stars (XDINSs[5]) and central compact objects (CCOs) in supernova remnants (SNRs) have been discovered. The X-ray emission of these NSs is pulsed, and the measured period derivatives are consistent with strong (a few times 10^{13} G) magnetic fields in XDINSs (Haberl 2007; Kaplan 2008) and relatively weak ($\lesssim 10^{11}$ G) magnetic fields in CCOs (Halpern & Gotthelf 2009). Therefore, the observed absorption features might be associated with ion cyclotron lines in XDINSs and electron cyclotron lines in CCOs. Correct identification of the observed features can provide important information on the chemical composition, magnetic field and gravitational redshift at the NS surfaces.

The most famous isolated NS with absorption features is 1E 1207.4–5209 (hereafter 1E 1207), which is the CCO of the PKS 1209–51/52 SNR, with properties similar to other CCOs (Pavlov et al. 2002, 2004; de Luca 2008; Halpern & Gotthelf 2009). Two absorption features in the spectrum of this isolated NS, centered at about 0.7 and 1.4 keV, were discovered by Sanwal et al. (2002) in *Chandra* observations, while later observations with *XMM-Newton* suggested the presence of two more features, at 2.1 and 2.8 keV (Bignami et al. 2003). The period $P = 0.424$ s was found by Zavlin et al. (2000) from X-ray pulsations. 1E 1207 shows a thermal-like X-ray spectrum with a black-body (BB) temperature ≈ 3 MK. The effective temperature $T_{\rm eff}$ may be substantially lower (≈ 1 MK) if the spectrum is formed in a hydrogen atmosphere (Zavlin et al. 1998).

It has been suggested that the harmonically spaced absorption features in 1E 1207 are the electron cyclotron line and its harmonics (Bignami et al. 2003). At first glance, one should not expect spectral features at harmonics of the cyclotron energy because in a classical (non-quantum) plasma the harmonics are due to relativistic effects (e.g., the ratio of emissivities and opacities in consecutive harmonics is $\sim kT/m_e c^2$ at $kT \gtrsim E_{c,e}$), which are very small in the relatively cold CCO atmospheres. However, Suleimanov et al. 2010 (hereafter SPW10) have demonstrated that, even in a cold plasma, harmonically spaced absorption lines can form due to quantum oscillations in the dependence of the free-free absorption on photon energy in a magnetic field (Pavlov & Panov 1976; see also a recent discussion of this process in Potekhin 2010). The peak energies of these oscillations coincide with the cyclotron energy and its harmonics, $E = sE_{c,e} = s\hbar eB/m_e c$ ($s = 1, 2, \ldots$). For 1E 1207, they correspond to the magnetic field $B_{\rm line} = 6 \times 10^{10}(E_{c,e}^{\infty}/0.7\,{\rm keV})(1 + z)$ G (z is the gravitational redshift in the NS surface layers), consistent with $B_{\rm sd} = 1 \times 10^{11}$ G, which corresponds to one of the two solutions obtained by Halpern & Gotthelf (2011) for the pulsar's period derivative[6].

The model atmospheres were calculated by SPW10 in the so-called cold plasma approximation (Ginzburg 1970), which implies, in particular, that effects associated with thermal motion of plasma particles can be neglected. All the previous

Electronic address:

[1] Institute for Astronomy and Astrophysics, Kepler Center for Astro and Particle Physics, Eberhard Karls University, Sand 1, 72076 Tübingen, Germany; suleimanov@astro.uni-tuebingen.de

[2] Dept. of Astronomy, Kazan Federal University, Kremlevskaya 18, 420008 Kazan, Russia

[3] Pennsylvania State University, 525 Davey Lab., University Park, PA 16802; pavlov@astro.psu.edu

[4] State Polytechnic University, Polytekhnicheskaya ul. 29, St.-Petersburg 195251, Russia

[5] These NSs are actually much brighter in X-rays than many other types of isolated NSs, but we will call them XDINSs following a historical tradition.

[6] This solution had been reported by Pavlov & Luna 2009 (see footnote #15 of that work).

magnetized NS atmosphere models, starting from the first work by Shibanov et al. (1992), have been calculated using this approximation. Without allowance for the above-mentioned quantum oscillations, there is only one resonance (the fundamental cyclotron resonance at $E = E_{c,e}$) in the electron component of the opacity of a fully ionized "cold" plasma, and this resonance occurs only in one polarization mode, called the extraordinary mode (X-mode), while the energy dependence of the opacity of the ordinary polarization mode (O-mode) remains smooth (see Pavlov et al. 1980a; hereafter PMS80). The thermal motion leads to the cyclotron resonance ($s = 1$) in the O-mode (Pavlov et al. 1979), to emission/absorbtion of the cyclotron harmonics ($s > 1$) in both polarization modes, and to the Doppler broadening of the cyclotron resonances (e.g., PMS80); the contribution of these processes is determined by the ratio $kT/m_e c^2$. In addition to the thermal effects, quantum relativistic effects (whose contribution is determined by the ratio $E_{c,e}/m_e c^2$, can be important when $E_{c,e} \gtrsim kT$ (Pavlov et al. 1980b; hereafter PSY80). These effects have been ignored in the NS atmosphere modeling because the parameter $\xi_e \equiv \max(kT, E_{c,e})/m_e c^2$ is small ($\sim 10^{-3}$) in atmospheres of isolated NSs. However, ξ_e is not the only parameter that determines the strengths of the cyclotron resonances. For instance, the depth of the cyclotron absorption features depends on the ratio of the peak opacity to the opacity in the neighboring continuum, which may be $\gg 1$ even for a very small ξ_e. Therefore, to properly interpret the spectral features observed in CCOs, one should use NS atmosphere models calculated with account for the thermal motion of electrons and quantization of the electron motion in a magnetic field.

Here we present first calculations of realistic magnetized NS atmosphere models with these effects taken into account. We show that the fundamental resonance in the O-mode and at least two harmonics in both polarization modes are significant in the emergent spectra at the effective temperatures and magnetic fields typical for CCOs. In particular, the thermal motion effects lead to formations of relatively deep Doppler cores at the centers of broad absorption features that arise due to quantum resonances in magnetic free-free absorption. These calculations demonstrate that the thermal motion and quantization must be taken into account for a quantitative description of the observed features in the spectra of CCOs.

2. OPACITIES IN ELECTRON CYCLOTRON LINE AND HARMONICS

Our consideration of the thermal cyclotron opacities is based on the works of PMS80 and PSY80, where simple approximate expressions for the cyclotron opacities were derived.

In PMS80, classic (non-quantum) relativistic opacities are considered with electron-ion collisions taken into account. According to that work, the shape of the cyclotron resonances can be described by the Voigt profile, which is the convolution of the Doppler and Lorentz profiles. For $\Gamma_D \gg \Gamma_c + \Gamma_r$ (where Γ_c, Γ_r and Γ_D are the collisional, radiative, and Doppler widths of the cyclotron resonances), the Voigt profile consists of a Doppler core, independent of Γ_c and Γ_r, and Lorentz wings, which are virtually unaffected by the thermal motion.

In the atmospheres considered in our work, the quantum effects are significant because $E_{c,e} \gtrsim kT_{\rm eff}$. The cyclotron absorption in the relativistic quantum case has been studied by PSY80 for a collisionless plasma. Since the free-free transitions, caused by electron-ion collisions, are not included in

that work (as well as in later works on thermal cyclotron processes in quantizing magnetic fields), the results of PSY80 are applicable only in Doppler cores of cyclotron harmonics. However, similar to PMS80, one can use the cold plasma approximation outside the Doppler cores (i.e., in the Lorentz wings and the continuum), because the relativistic corrections are negligible there (at $kT_e \ll m_e c^2$). Moreover, since the thermal cyclotron opacity in the Doppler cores is much larger than the free-free opacity (except for the fundamental resonance in X-mode), and the thermal cyclotron opacity decreases exponentially in the wings of the resonances, one can calculate the total opacity as the sum of these two (see Figure 1 in PMS80). Therefore, we use the following approach in our calculations. For each used photon energy E, we calculate separately the opacities in the cold plasma approximation, with the quantum oscillations in the magnetic free-free opacities taken into account (see details in Suleimanov et al. 2009 and SPW10), and the cyclotron opacities (with quantum effects taken into account) in the collisionless approximation (PSY80). Then, we simply add the collisionless opacities at all the harmonics (except for the fundamental resonance in X-mode) to the magnetic free-free opacities in the corresponding modes. For the fundamental resonance in X-mode, we compare the two opacities and take the larger one as the actual opacity at this energy. The used approach only slightly distorts the frequency dependence of the absorption coefficients in the transition regions between the cores and the wings, but this should not significantly affect the emergent spectrum because this transition occurs at different distances from the cyclotron resonances at different depths.

We perform all calculations in the local thermodynamic equilibrium (LTE) approximation. This means that the cyclotron absorption is considered as a "true absorption", without scattering, and the cyclotron absorption does not contribute to the scattering part of the source function in the radiative transfer equations, which take into account the coherent electron scattering in the continuum only.

The approximate equations that we use to compute the cyclotron opacities are presented below (see PSY80 for details). They are not sufficiently accurate at angles θ between the magnetic field and the photon wave vector close to $90°$, i.e., at $|\cos\theta| \lesssim \beta$, where β is the ratio of the thermal velocity v_T to the speed of light:

$$\beta = \frac{v_T}{c} = \left(\frac{2kT}{m_e c^2} \right)^{1/2}. \qquad (1)$$

As only a small amount of radiation is transferred at these angles, we exclude them from our code and extrapolate the radiation field properties into this angle range.

We calculate the opacities k_j (cm^2 g^{-1}) for polarization modes $j=1$ (X-mode) and $j = 2$ (O-mode). The opacity k_j is proportional to the imaginary part, κ_j, of the complex refraction coefficient:

$$k_j = \frac{4\pi\nu}{c\rho} \kappa_j, \qquad (2)$$

where ν is photon frequency and ρ plasma density. We present equations for κ_j below.

An example of the computed continuum opacities, together with the opacities at the cyclotron line and its harmonics, is shown in Figure 1 for various θ. Notice that, at some angles, the opacities at the fundamental resonance and first two harmonics are larger than the continuum opacities in both modes.
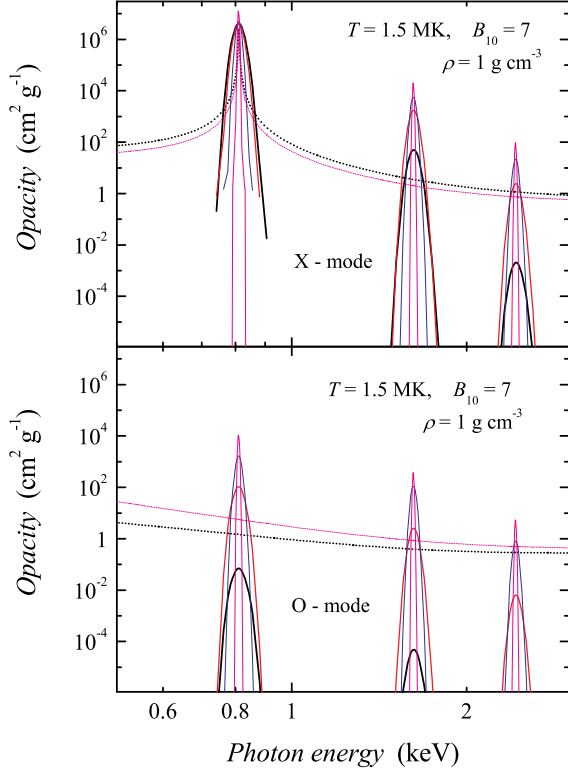
Figure 1. Opacities in cyclotron lines and continuum opacities in two polarization modes (top and bottom panels) in a magnetized plasma with $T = 1.5$ MK, $\rho = 1$ g cm^{-3}, and $B = 7 \times 10^{10}$ G, for four values of the angle θ between the magnetic field and the photon wave vector: 5° (thickest black curves), 30° (thick red curves), 60° (thin blue curves), and 80° (thinnest magenta curves). Continuum opacities for two values of θ are shown by dotted curves (thick black curves for $\theta = 5°$ and thin magenta curves for 80°).

This allows one to expect significant absorption lines at these resonances in the emergent spectra of magnetized NS model atmospheres.

2.1. Opacities at the fundamental electron cyclotron resonance

According to PSY80, the equations for the normal mode opacities near the fundamental resonance are qualitatively different in the regimes of weak and strong vacuum polarization by magnetic field, i.e., at small and large values of the parameter $V\beta\cos\theta\sin^2\theta$, where

$$V = \frac{3 \times 10^{28}\,\text{cm}^{-3}}{n_e}\left(\frac{B}{B_Q}\right)^4,\qquad(3)$$

n_e is the electron number density, B the magnetic field strength, and $B_Q = 4.414 \times 10^{13}$ G is the magnetic field at which $E_{c,e} = m_e c^2$. In the case of CCOs, with their relatively weak magnetic fields, the regime of weak vacuum polarization is applicable throughout the NS atmosphere. In this regime, the vacuum polarization does not affect the X-mode opacity:

$$\kappa_1 \approx \frac{\nu_p^2}{\nu^2}\frac{1 + \cos^2\theta}{4\beta|\cos\theta|}\sqrt{\pi}\,\exp(-x_1^2).\qquad(4)$$

Here $h\nu = E$ is the photon energy, and ν_p is the electron plasma frequency,

$$\nu_p^2 = \frac{e^2 n_e}{\pi m_e}.\qquad(5)$$

The dimensionless energy shift x_s relative to the central resonance energy in the s-th harmonic ($s = 1$ corresponds to the fundamental resonance) is defined by the following expression

$$x_s = \frac{\xi - sb + s^2\beta^2 b^2/4}{\varkappa} - \frac{\varkappa}{4},\qquad(6)$$

where

$$b = \frac{h\nu_B}{kT},\quad h\nu_B = E_{c,e},\quad \xi = \frac{h\nu}{kT},\qquad(7)$$

$$\varkappa = h\nu\left(\frac{2}{m_e c^2\,kT}\right)^{1/2}|\cos\theta|.$$

In the same regime, the O-mode opacity is given by the following equation:

$$\kappa_2 = \frac{\nu_p^2}{\nu^2}\frac{\beta\sin^4\theta\sqrt{\pi}}{4(1 + \cos^2\theta)|\cos\theta|}\left[\frac{b}{4}\tanh\frac{b}{2} + \right.\qquad(8)$$

$$\left.\frac{(3 + \tan^2\theta - 2V)^2}{\pi(1 + \cos^2\theta)^2(H_1^2 + F_1^2)}\cos^4\theta\right]\exp(-x_1^2).$$

Here $H_s \equiv H(x_s)$ and $F_s \equiv F(x_s)$ are the real and imaginary parts of the plasma dispersion function $W(x_s)$:

$$W(z) = H(z) + iF(z) = \frac{i}{\pi}\int_{-\infty}^{+\infty}\frac{e^{-u^2}}{z - u}\,du.\qquad(9)$$

$H(z)$ is the well-known Voigt function, proportional to the Doppler profile in our approximation,

$$H(x + iy) = \frac{y}{\pi}\int_{-\infty}^{+\infty}\frac{e^{-u^2}}{(x - u)^2 + y^2}\,du \xrightarrow{y \to 0} e^{-x^2},\quad(10)$$

while $F(z)$ is its Hilbert transform:

$$F(x + iy) = \frac{1}{\pi}\int_{-\infty}^{+\infty}\frac{e^{-u^2}(x - u)}{(x - u)^2 + y^2}\,du\qquad(11)$$

$$\xrightarrow{y \to 0}\frac{1}{\pi}\int_{-\infty}^{+\infty}\frac{e^{-u^2}}{x - u}\,du.$$

2.2. Opacities in higher harmonics

The values of κ_j in the harmonics $s > 1$ are given by the following equation (signs "plus" and "minus" correspond to X-mode and O-mode, respectively):

$$\kappa_j = \frac{\nu_p^2}{\nu^2}A\,(X \pm Y)\exp(-x_s^2),\qquad(12)$$

where

$$X = 1 + \cos^2\theta + \zeta\sin^2\theta,\qquad(13)$$

$$Y = (1 + G^2)^{-1/2}\left[2|\cos\theta| + G(1 - \zeta)\sin^2\theta\right],\quad(14)$$

$$G = \frac{\sin^2\theta}{2|\cos\theta|}\frac{\nu_B^4 + V\nu^2(\nu^2 - \nu_B^2)}{\nu_B^3\nu},\qquad(15)$$

$$\zeta = \frac{\xi^2\beta^2\sin^2\theta}{4sb}\tanh\frac{b}{2},\qquad(16)$$

$$A = \frac{1}{8} \left(\frac{b}{1 - e^{-b}} \right)^s \frac{1 - e^{-\xi}}{\xi} \frac{s}{(s-1)!} \times \qquad (17)$$
$$\frac{\sqrt{\pi}}{\beta |\cos\theta|} \left(\frac{\beta\nu\sin\theta}{2\nu_B} \right)^{2s-2} .$$

3. ATMOSPHERE MODELS

We calculate the magnetic hydrogen atmosphere models using our recently developed code (Suleimanov et al. 2009; SPW10), assuming the magnetic field normal to the stellar surface. We also assume that the atmosphere is fully ionized because, in the relatively low magnetic fields considered here, and temperatures of a few million Kelvin, the fraction of bound species in a hydrogen atmosphere is very low (see, e.g., Pavlov et al. 1995). Moreover, all the hydrogen lines and photoionization jumps lie in far (or extreme) ultraviolet, unobservable because of the interstellar absorption (e.g., the energy of the strongest hydrogen line at $B = 10^{11}$ G is about 26 eV, while the photoionization energy of the ground state is about 78 eV; see Roesner et al. 1984). Therefore, atomic lines are unobservable in CCOs, and bound species do not make a strong effect on the temperature run and the emergent spectrum.

We calculated two sets of atmosphere models with the same parameters as in SPW10. The surface gravitational acceleration $g = 10^{14}$ cm s^{-2} for all the models. In the first set we fixed the magnetic field strength ($B = 7 \times 10^{10}$ G) and computed models with three different effective temperatures, $T_{\rm eff} = 1$, 1.5, and 3 MK. The emergent flux spectra and temperature structures for the models computed with and without the collisionless cyclotron opacities are shown in Figure 2. A common property of the emergent spectra for the models with the cyclotron opacities are prominent absorption cores at the cyclotron energy and its harmonics, $E_s = sE_{c,e} = 0.81 s$ keV ($s = 1, 2, \ldots$), in addition to the wide absorption wings caused by the quantum oscillations in the magnetic free-free opacities in the cold plasma approximation (SPW10). The equivalent width w_s of the s-th absorption feature decreases with increasing s as well as with increasing $T_{\rm eff}$ (i.e., with decreasing the effective quantization parameter, $b_{\rm eff} \equiv E_{c,e}/kT_{\rm eff} \approx 9.4$, 6.3, and 3.1 for the three models). However, these dependences are weaker than in the models computed in the cold plasma approximation. For instance, $w_1 = 243$ (240), 213 (200), and 213 (180) eV at $T_{\rm eff} = 1$, 1.5, and 3 MK, respectively, while $w_2 = 234$ (190), 205 (140) and 146 (55) eV at the same temperatures, where the numbers in parentheses are equivalent widths for the models calculated in the cold plasma approximation.

The second set consists of four models with different magnetic field strengths ($B = 1$, 4, 7, and 10 $\times 10^{10}$ G) at the same effective temperature, $T_{\rm eff} = 1.5$ MK. The comparison of the emergent spectral fluxes for the models calculated with and without thermal cyclotron opacities is shown in the top panel of Figure 3. Again, the equivalent widths of the absorption features decrease with increasing harmonic number and decreasing magnetic field strength. The difference of the emergent spectra computed with and without thermal cyclotron opacities is similar to that seen in Figure 2. In particular, the new models show substantially deeper cores of the absorption features at the cyclotron energy and its harmonics, while the continuum spectra remain virtually the same.
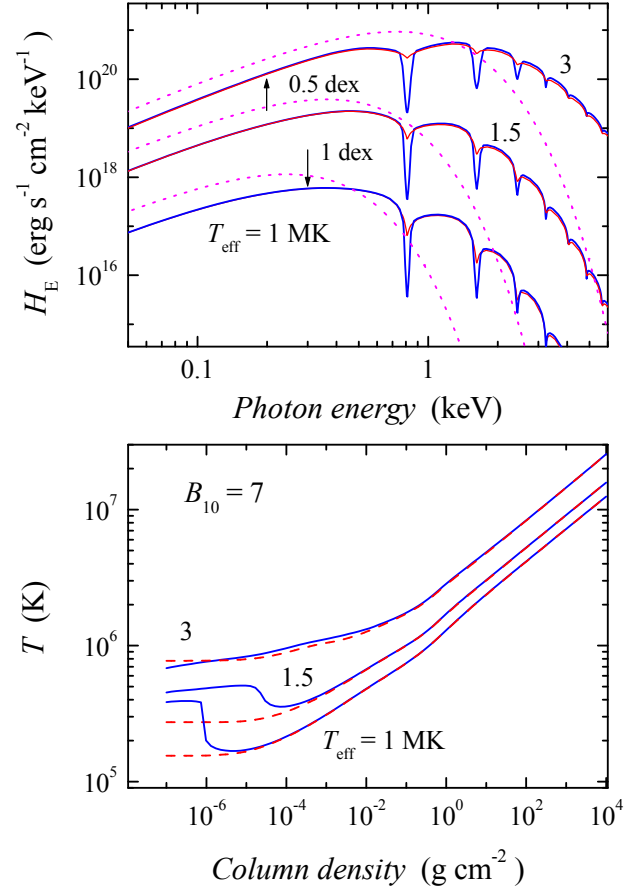
The bottom panel of Figure 4 shows spectra of emergent

Figure 2. *Top panel:* Emergent flux spectra for magnetic NS atmospheres ($B = 7 \times 10^{10}$ G) in the cold plasma approximation (thin solid lines) and with the collisionless cyclotron opacities included (thick solid curves) for three effective temperatures, $T_{\rm eff} = 1$, 1.5, and 3 MK. For clarity, the spectra for $T_{\rm eff} = 3$ and 1 MK are shifted along the ordinate axis by factors $10^{+0.5}$ and 10^{-1}, respectively. The dotted curves show blackbody spectra for the same temperatures. *Bottom panel:* Temperature structures for the same models. Solid curves correspond to the models with collisionless cyclotron opacities included, dashed curves to the models in the cold plasma approximation. Notice the overheating of the outer layers in the models with the collisionless cyclotron opacities included.

specific intensity for the model with $T_{\rm eff} = 1.5$ MK and $B = 7 \times 10^{10}$ G, for various angles θ between the line of sight and the normal to the surface. The quantum oscillations together with deep cyclotron cores in the intensity spectra are seen at any angle. The cyclotron cores depend on θ stronger than the quantum oscillation wings. They are virtually invisible at small angles, in accordance with the disappearance of thermal cyclotron resonances at $\theta \to 0$ in the O-mode for $s = 1$ and both modes for $s > 1$ — see Equations (8) and (17), and they become narrower and deeper with increasing θ. The equivalent width of the absorption feature at the fundamental resonance depends on θ non-monotonously. For instance, $w_1 \simeq 228$ (220), 180 (160), 380 (320) and 400 (330) eV for $\theta = 5°$, 30°, 60° and 80°, respectively (the equivalent widths calculated in the cold plasma approximation are in parentheses).

In the top panel of the same Figure 4, the angular distributions of the emergent intensity at five photon energies (near the fundamental resonance, the first harmonic, and three con-
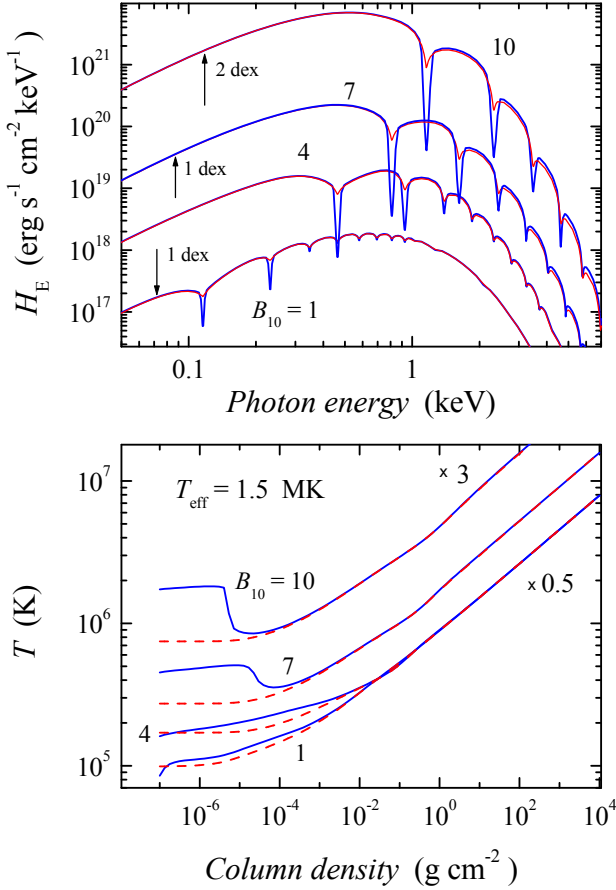
Figure 3. *Top panel:* Emergent spectral fluxes for atmospheres with $T_{\rm eff} = 1.5$ MK and magnetic fields $B = 1, 4, 7$ and 10×10^{10} G, calculated with and without including the collisionless cyclotron opacities (thick and and thin solid lines, respectively). For clarity, the spectra for $B_{10} = 10, 7$ and 1 are shifted along the ordinate axis by factors $10^{+2}, 10^{+1}$ and 10^{-1}, respectively. *Bottom panel:* Temperature structures for models with and without the cyclotron opacities (solid and dashed curves, respectively), for the same parameters. For clarity, the temperature structures for $B_{10} = 10, 4$ and 1 are shifted along the ordinate axis by factors 3, 0.5 and 0.5, respectively.

Figure 4. *Top panel:* Angular distribution of the emergent specific intensity at the fundamental resonance, first harmonic ($s = 2$), and three continuum photon energies (indicated in the plot) for a NS atmosphere with $B = 7 \times 10^{10}$ G, $T_{\rm eff} = 1.5$ MK. *Bottom panel:* Spectra of the emergent specific intensity for the same model at different angles to the surface normal (indicated in the plot).

tinuum energies) are shown. Unlike the absorption features arising in the cold plasma approximation (see SPW10), the specific intensities at the cyclotron cores are stronger peaked towards the surface normal (i.e., towards the magnetic field direction) than those in the continuum.

Spectra of emergent specific intensity in the O- and X-modes, for the model with the same parameters as in Figure 4, are shown in Figure 5. The intensity spectra in the X-mode depend on θ only slightly (bottom panel), while the intensity spectra in the O-mode, which dominates at $E \gtrsim E_{c,e}$, vary with θ similar to the intensity summed over polarizations (cf. Figure 4).

The bottom panels of Figures 2 and 3 show the temperature structures for the six atmosphere models in comparison with the temperature structures of the corresponding models computed in the cold plasma approximation. The main effect of the thermal cyclotron transitions is the temperature rise in outer atmospheric layers, caused by an additional cyclotron heating due to the resonance in the O-mode opacity.

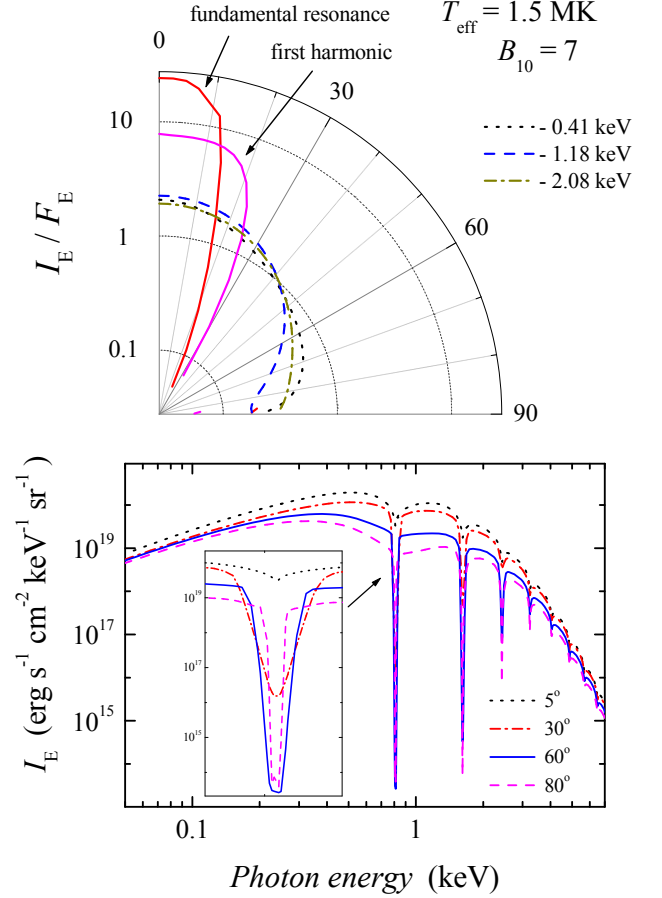The depths of the spectrum formation (the column densities

which correspond to $\tau_E^i = 1$) for the new model are shown in Figure 6. We see that in the region of cyclotron harmonics the O-mode comes from deeper (hotter) layers than the X-mode. Since these layers are much deeper than the outer layers overheated by the cyclotron absorption (see Figures 2 and 3), the overheating does not affect the emergent radiation summed over polarizations.

We also computed the radiative acceleration $g_{\rm rad}$, which is defined by the following equation

$$g_{\rm rad} = \frac{2\pi}{c} \sum_{i=1}^{2} \int_0^\infty d\nu \int_{-1}^{+1} (k_\nu^i + \sigma_\nu^i)\, \mu\, I_\nu^i(\mu)\, d\mu, \quad (18)$$

where $\mu = \cos\theta$. The calculated $g_{\rm rad}$ values are smaller than the surface gravity for all the computed model atmospheres (Figure 7) and can be ignored.

The vacuum polarization by the magnetic field might be significant in outer atmosphere layers, where the electron number density is very low. We have checked, however, that including the vacuum polarization into the calculations only slightly changes the temperature structure and the radiative acceleration at the very surface (Figure 8), and it does not change the emergent spectrum at all. In the top panel of
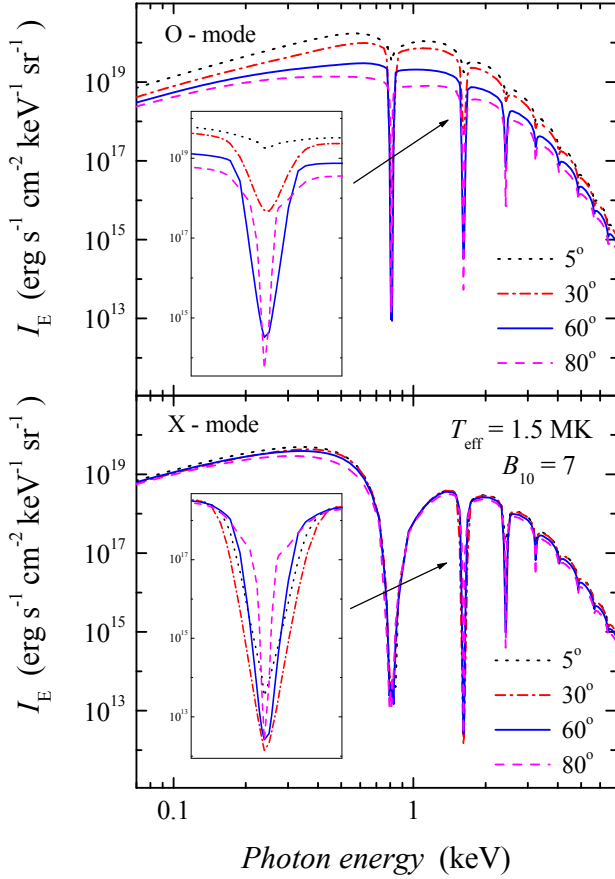
Figure 5. Spectra of the emergent specific intensity in the O-mode (top panel) and X-mode (bottom panel) for the same atmosphere model as in Figure 4, at different angles to the surface normal (indicated in the plot).

the same figure, the radiation pressure distributions in the atmospheres are also shown, and the agreement with the equilibrium thermodynamic value in the optically thick layers is demonstrated.

4. DISCUSSION

We have presented the first computations of fully ionized hydrogen atmospheres of NSs for magnetic fields $B \sim 10^{10}$–10^{11} G without using the cold plasma approximation. For the magnetic fields chosen, the electron cyclotron energy, $E_{c,e} \sim 0.1$–1 keV, is within the range of energies where the thermal emission from isolated NSs is usually observed. We have shown that the thermal effects lead to formation of deep Doppler cores in the absorption features at the cyclotron energy and its harmonics, and to a sharper angular dependence of the emergent intensity at the cyclotron features. The main contribution to the equivalent widths of the cyclotron features still comes from the feature wings, which are due to the quantum oscillations in the magnetic free-free opacity and can be considered in the cold plasma approximation. However, the contribution of the Doppler cores is significant, and it increases with increasing the quantization parameter b_{eff} and the harmonic number. The equivalent widths of the features reach $\sim$ 150–250 eV in the examples considered; they grow with increasing b_{eff} and are lower for higher harmonics.

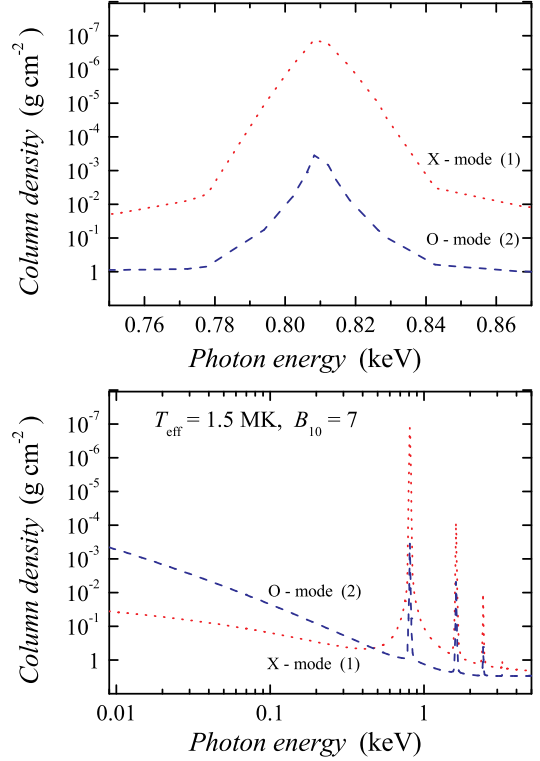In our previous work (SPW10) we suggested that the har-

Figure 6. Photon energy versus flux formation depth (column density corresponding to τ_E^i =1) in the O- and X-modes for the atmosphere with $T_{\text{eff}} = 1.5$ MK, $B_{10} = 7$. In the top panel the energy band around the fundamental resonance is shown in more detail.

monically spaced absorption features in the X-ray spectrum of the CCO 1E 1207 (Sanwal et al. 2002, Bignami et al. 2003) are due to the quantum oscillations in the magnetic free-free opacity. We ignored the relativistic effects, such as the thermal cyclotron processes, because the thermal and cyclotron energies are essentially nonrelativistic for 1E 1207 ($kT_{\text{eff}}/m_e c^2 < E_{c,e}/m_e c^2 \sim 10^{-3}$). However, the detailed study presented here has demonstrated that these effects are important and must be included in the model atmosphere calculations. The reason is the large ratios of the cyclotron resonance opacities to the continuum opacity (e.g., $\sim 10^4$ and $\sim 10^1$ for the $s = 2$ and $s = 3$ harmonics, respectively, for the atmosphere parameters relevant to the case of 1E 1207). Therefore, the inclusion of the thermal cyclotron opacities in modeling atmospheres of 1E 1207 and similar objects is needed.

In future work we plan to compare the model spectra obtained by integrating the specific intensities over the visible NS surface (at different rotation phases and for various orientations of the rotation and magnetic axes) with the phase-dependent spectra of 1E 1207 to infer the properties of this NS. The integration should lead to a broadening of cyclotron features because of the nonuniformity of the surface magnetic field, without dramatic changes of equivalent widths. We note that the pulsations detected in the radiation of 1E 1207 are strong only in the spectral features, and we believe that the strong angular dependence of the modeled emergent intensity in the cores of cyclotron harmonics (see Figures 4 and 5) can explain this fact and provide a potentially powerful tool for the determination of the NS parameters.
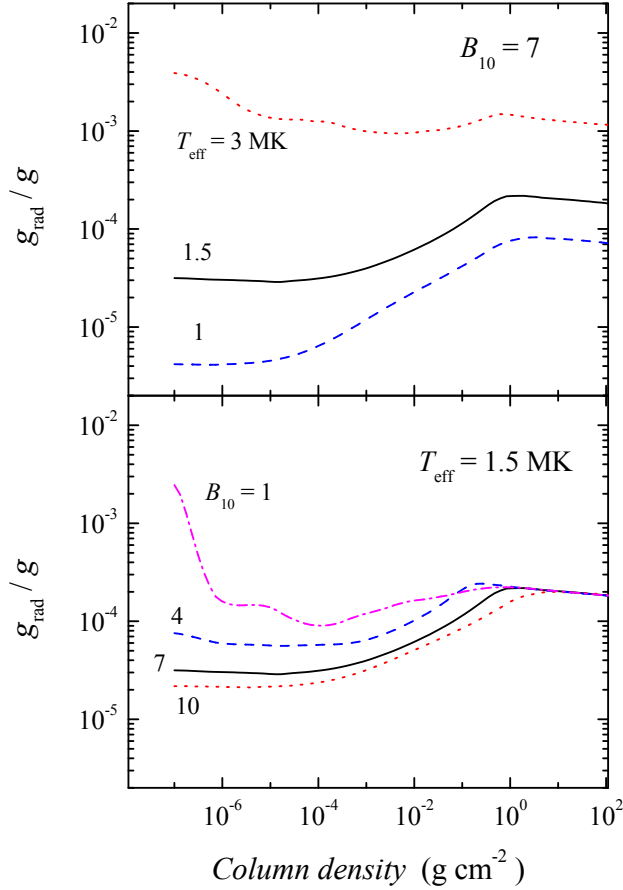
Figure 7. Relative radiation accelerations in all the computed model atmospheres (see Figs. 2 and 3). The atmosphere parameters are indicated in the panels.

Figure 8. Comparison of temperature structures (bottom panel) and relative accelerations due to radiation pressure (top panel) for models with (dashed curves) and without (solid curves) vacuum polarization taken into account. In the top panel, the corresponding radiation pressures are also shown.

In SPW10 we discussed the importance of quantum oscillations in the magnetic free-free opacity for the interpretation of the X-ray spectra of some other CCOs (J1852+0040 in the Kesteven 79 SNR and J0822–4300 in the Puppis A SNR) and low-field radio pulsars. It is clear that the thermal cyclotron processes may also be significant for these objects and must be included in calculations of their model atmospheres.

In the X-ray spectra of XDINSs, whose magnetic field are 2–3 orders of magnitude higher than in CCOs, proton (or ion) cyclotron lines are probably observed. The thermal cyclotron processes should be less important for ions because the parameter $\xi_p \equiv \max(kT, E_{c,p})/m_p c^2$ is at least three orders of magnitude smaller than ξ_e, and the Doppler width of the ion cyclotron resonance is ≈ 40 times smaller. However, the ratio of the ion resonance cyclotron opacity to the continuum opacity is also large for atmospheres of these NSs ($\gtrsim 10^7$, see, e.g. Figs. 2 and 4 in Suleimanov et al. 2009). Therefore, a contribution of the ion cyclotron harmonics to the emergent XDINS model spectra cannot be excluded and have to be investigated[7].

In the model atmospheres computed here, the radiation transfer calculations were performed using the LTE approx-

imation. Therefore, the source functions at the cyclotron line and its harmonics were taken equal to the Planck function, and the photon scattering in the cyclotron resonances was ignored. For a more accurate consideration, one should include non-coherent photon scattering in the cyclotron resonances. This is not simple (see, for example, Nagel 1981), and it has never been considered self-consistently. We plan to develop magnetized atmosphere models with non-coherent photon scattering in the cyclotron line and its harmonics in future work.

REFERENCES

Bignami, C. F., Caraveo, P. A., De Luca, A., & Mereghetti, S. 2003, Nature, 423, 725
De Luca, A. 2008, in AIP Conf. Proc. 983, 40 Years of Pulsars: Millisecond Pulsars, Magnetars and More, ed. C. Bassa et al. (Melville, NY: AIP), 311
Ginzburg, V. L. 1970, The Propagation of Electromagnetic Waves in Plasmas (Oxford: Pergamon)
Haberl, F. 2007, Ap&SS, 308, 181

[7] Here we mean the thermal Doppler cores of the ion cyclotron harmonics, not the small quantum peaks in the magnetic free-free opacities (see Potekhin 2010 and references therein).
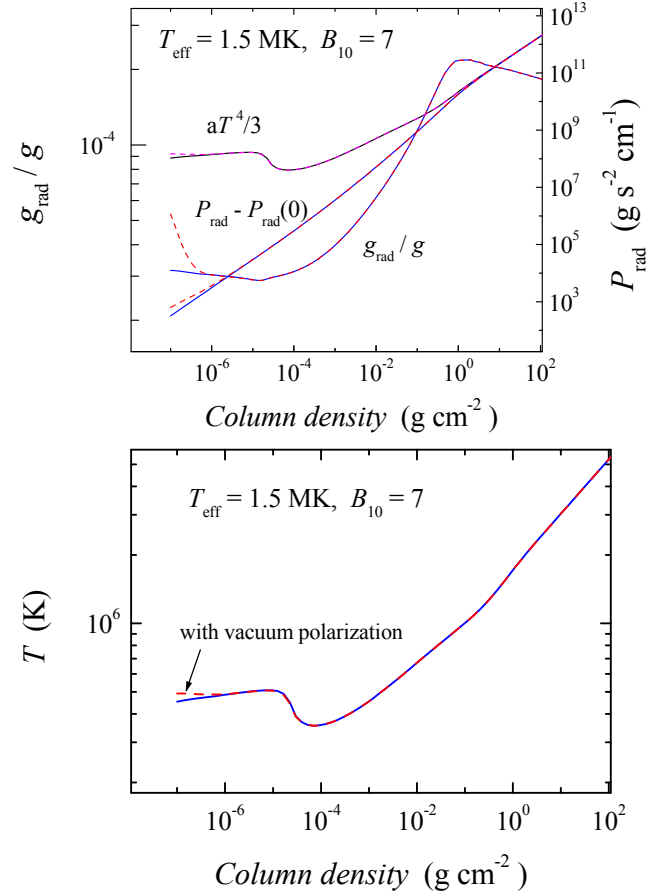
Halpern, J. P., & Gotthelf, E. F. 2009, ApJ, 709, 436
Halpern, J. P., & Gotthelf, E. F. 2011, ApJ, 733, L28
Kaplan, D. L. 2008, in AIP Conf. Proc. 983, 40 Years of Pulsars:
     Millisecond Pulsars, Magnetars, and More, ed. C. G. Bassa et al.
     (Melville, NY: AIP), 331
Nagel, W. 1981, ApJ, 251, 288
Pavlov, G. G., & Luna, G. J. M. 2009, ApJ, 703, 910
Pavlov, G. G., Mitrofanov, I. G., & Shibanov, Yu. A. 1980a, Ap&SS, 73, 63
     (PMS80)
Pavlov, G. G., & Panov, A. N. 1976, Sov. Phys. JETP, 44, 300
Pavlov, G. G., Sanwal, D., Garmire, G. P., & Zavlin, V. E. 2002, in ASP
     Conf. Ser. 271, Neutron Stars in Supernova Remnants, ed. P. O. Slane &
     B. Gaensler (San Francisco, CA: ASP), 247
Pavlov, G. G., Sanwal, D., & Teter, M. A. 2004, In IAU Symp. 218, Young
     Neutron Stars and Their Enviroments, ed. F. Camilo & B. Gaensler (San
     Francisco, CA: ASP), 239
Pavlov, G. G., Shibanov, Yu. A., & Gnedin, Yu. A. 1979, JETP Lett., 30, 125
Pavlov, G. G., Shibanov, Yu. A., & Yakovlev, D. G. 1980b, Ap&SS, 73, 33
     (PSY80)

Pavlov, G. G., Shibanov, Yu. A., Zavlin, V. E., & Meyer, R. D. 1995, in The
     Lives of the Neutron Stars, eds. M. A. Alpar, Ü. Kiziloğlu, & J. van
     Paradijs (Kluwer: Dordrecht), 71
Potekhin, A.Y. 2010, A&A, 518, A24
Roesner, W., Wunner, G., Herold, H., & Ruder, H. 1984, Journal of Physics
     B, 17, 29
Sanwal, D., Pavlov, G. G., Zavlin, V. E., & Teter, M. A. 2002, ApJ, 574, L61
Shibanov, Yu. A., Zavlin, V. E., Pavlov, G. G., & Ventura, J. 1992, A&A,
     266, 313
Suleimanov, V. F., Potekhin, A. Y., & Werner, K. 2009, A&A, 500, 891
Suleimanov, V. F., Pavlov, G. G., & Werner, K. 2010, ApJ, 714, 630
     (SPW10)
Zavlin, V. E., Pavlov, G. G., & Trümper, J. 1998, A&A, 331, 821
Zavlin, V. E., Pavlov, G. G., Sanwal, D., & Trümper, J. 2000, ApJ, 540, L25